

PROBLEM NO. FAC-2

Title: Predicting Residual Strength of a Fuselage Section with/without MSD and with/without Corrosion

Objective

To illustrate the process of using the nonlinear finite element method to evaluate the residual strength of a built-up aircraft structure possibly containing multi-site fatigue damage and possibly having corrosion damage.

General Description:

This problem details the process of using the finite element method to predict the residual strength of a section of built-up fuselage structure. The section contains a lead fatigue crack, and might also contain MSD and corrosion damage. Stable growth of the lead crack is simulated based on the critical crack tip opening angle (CTOA_c) criterion. Methods for representing rivet stiffness and for local meshing are described. The process is applied to a section of K/C-135 fuselage, and strength assessment curves are generated for a number of configurations with no MSD, with MSD, and with MSD and corrosion conditions.

Topics Covered: Finite element analysis, stable tearing, MSD, corrosion damage, residual strength, non-linear fracture mechanics

Type of Structure: section of K/C-135 fuselage

Relevant Sections of Handbook: Sections 2, 4, 5, 11

Author: Dr. A. R. Ingraffea

Company Name: Fracture Analysis Consultants, Inc.

121 Eastern Heights Drive
Ithaca, NY 14850
607-257-4970
www.fracanalysis.com

Contact Point: Dr. Paul Wawrzynek

Phone: 607-257-4970

e-Mail: wash@fracanalysis.com

Fracture Analysis
Consultants, Inc.

Overview of Problem Description

A relatively simple built-up narrow body fuselage configuration is modeled. The example demonstrates an analysis to predict the residual strength of a pressurized fuselage, subjected to MSD and corrosion damage [Cope 1998]. The problem chosen for analysis is a three stringer wide, three-frame long K/C-135 fuselage panel. The panel section has a radius of curvature of 72 inches. It contains a lap joint at the central stringer. The lap joint is a typical three-row configuration with 3/16 inch diameter countersunk rivets. The other two stringers are spot-welded to the skin. The upper and lower skins are made of 0.04 inch thick, 2024-T3 aluminum alloy. The stringers and frames are made of 7075-T6 aluminum alloy. Frames are simply connected to the stringers by rivets. The panel configurations are shown in [Figures FAC-2.1](#) and [FAC-2.2](#). The frame and stringer dimensions are shown in [Figure FAC-2.3](#).

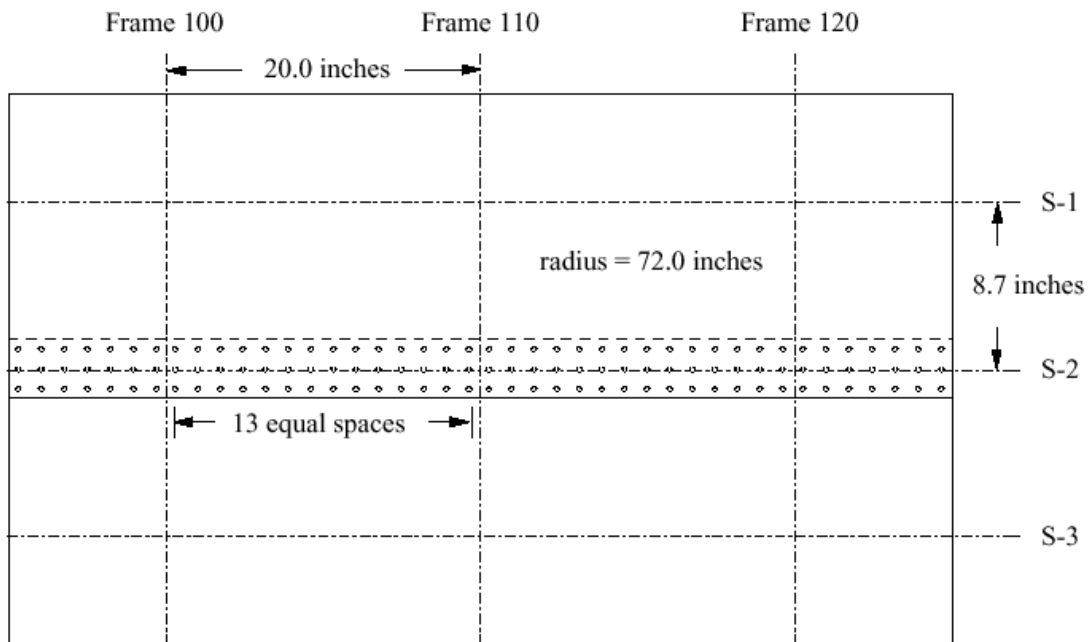


Figure FAC-2.1. Layout of K/C-135 fuselage section used in the present example.

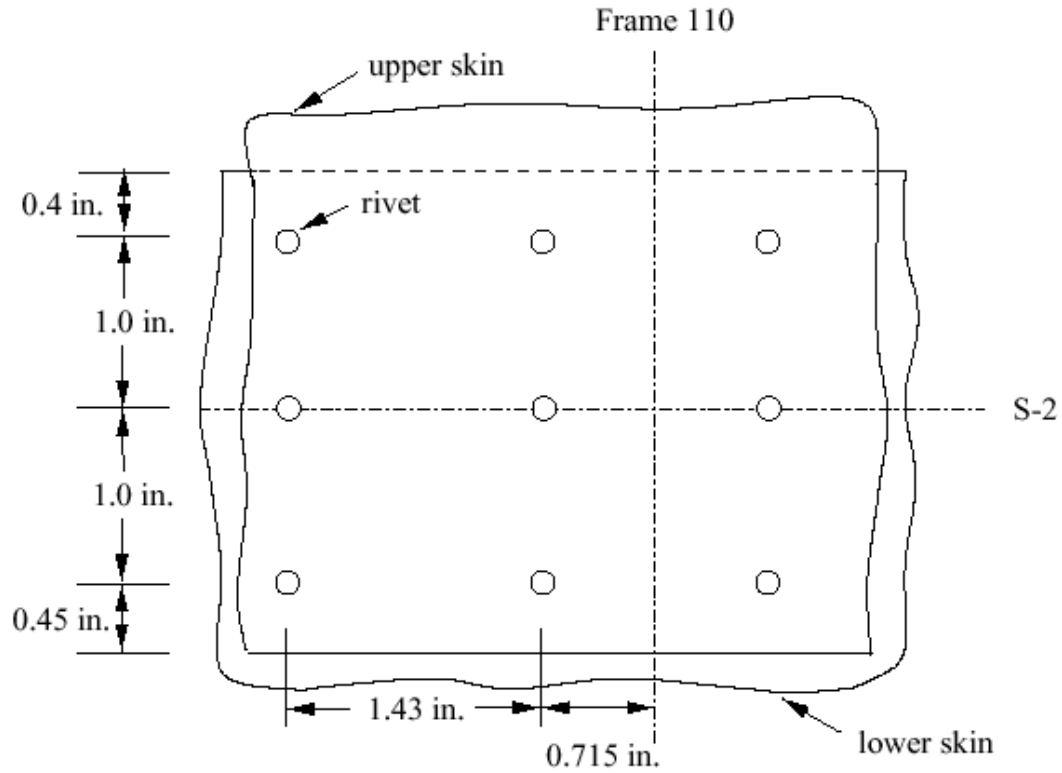


Figure FAC-2.2. Detail of lap joint rivet spacing used in the present example.

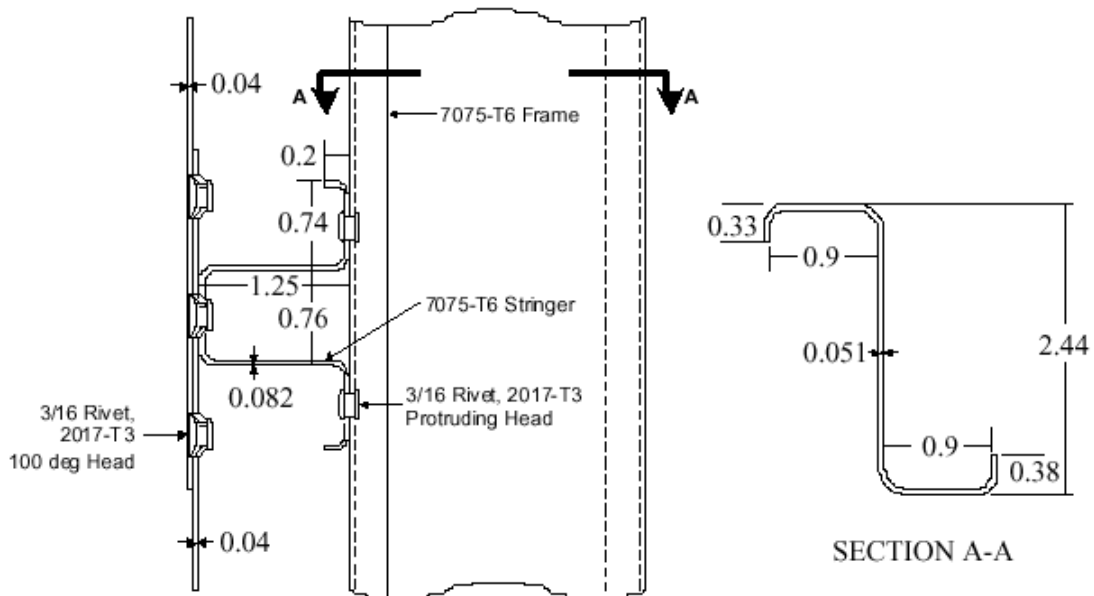


Figure FAC-2.3. Dimensions (all in inches) of stringer and frame used in the present example.

Computational Model

All structural components including skins, stringers, and frames are modeled by displacement-based, four-noded or five-noded Kirchoff shell finite elements [Rankin 1991]. The geometrical and mesh models were created using FRANC3D [www.cfg.cornell.edu], and all finite element computations were performed with STAGS [Rankin 1997]. Each node of a shell element has six degrees of freedom. A piecewise linear representation is used for the uniaxial stress-strain curves for 2024-T3 and 7075-T6 aluminum alloys (see [Figures FAC-2.4](#) and [FAC-2.5](#)).

Symmetric boundary conditions are imposed on all the boundary edges to simulate a cylinder-like fuselage structure. Pressure loading is applied on all the external skins. Uniform axial expansion was allowed at one longitudinal end. On this boundary edge, an axial force equal to $(PR/2)L$ was assigned where P is the applied pressure, R is the radius of the panel, and L is the arc-length of the edge. The kinematic boundary conditions (displacements and rotations) applied along the boundaries of this local model were extracted from a global model of the fuselage. Both geometric and material nonlinearities are included in the analysis. The former captures the out-of-plane bulging deformation and the latter captures the active plastic zone and the plastic wake during stable crack propagation.

The nonlinear solution algorithm consists of Newton's method. Large rotations are included in the nonlinear solution by a co-rotation algorithm applied at the element level [Nour-Omid 1991]. The Riks arc-length path following method is used to trace a solution past the limit points of a nonlinear response [Rankin 1997; Riks 1984].

Rivets are modeled by elastic-plastic spring elements that connect finite element nodes in the upper and lower skins. Each rivet is modeled with six degrees-of-freedom, corresponding to extension, shearing, bending and twisting of the rivet. The stiffness of each degree-of-freedom is defined by prescribing a force-deflection curve. The axial, flexural, and torsional stiffnesses of the spring elements are computed by assuming that the rivet behaves like a simple elastic rod with a diameter of 3/16 inch. The elastic shear stiffness of the rivet is computed by the following empirical relation developed by Swift [1984]:

$$K_{rivet} = \frac{ED}{[A + C(\frac{D}{t_1} + \frac{D}{t_2})]}$$

where E is the elastic modulus of the sheet material, D is the rivet diameter, t_1 and t_2 are the thicknesses of the joined sheets, and $A = 5.0$ and $C = 0.8$ for aluminum rivets. The initial shear yielding and ultimate shear strength of the rivets are assumed to occur at load levels of 510 lb and 725 lb, respectively. Once a rivet reaches its ultimate strength, it will break and lose its load carrying capacity. The force-deflection curve shown in [Figure FAC-2.6](#) for shearing is intended to represent empirically the net shear stiffness of a

riveted sheet connection, accounting for bearing deformations and local yielding around the rivet [Young 1997; Swift 1984].

The critical crack tip opening angle (CTOA_c) [Dawicke 1994] is used to characterize elastic-plastic crack growth and to predict residual strength. For details on use of this criterion, see Problem FAC-4. The CTOA_c used in this example was 5.7 degrees measured 0.04 inch behind the crack tip with a plane strain core height equal to 0.08 inch [Dawicke 1997]. Since no experimental crack growth data are available for this structure, this particular CTOA_c value is estimated based on the 5.25 degrees found for 0.09 inch thick, 2024-T3 bare material. The plane strain core height is assumed to be twice the sheet thickness.

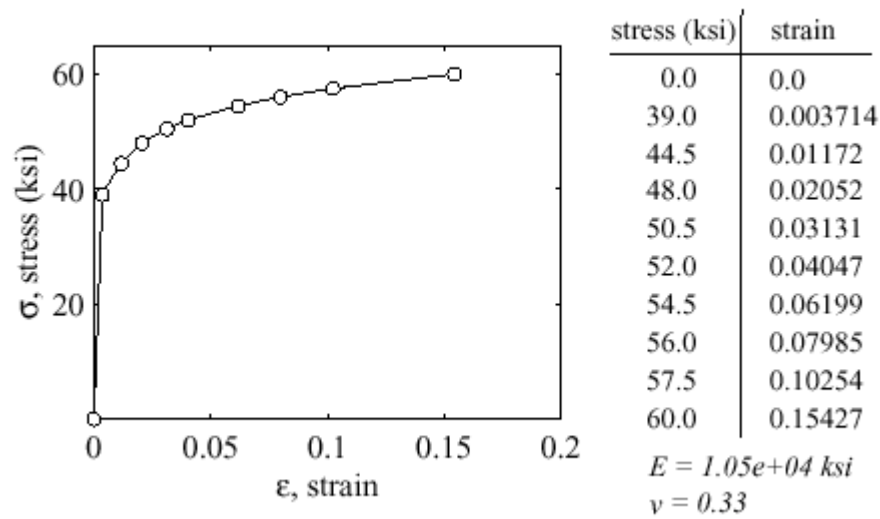


Figure FAC-2.4. Piecewise linear representation of uniaxial stress-strain relationship for 2023-T3 aluminum alloy used in the present example.

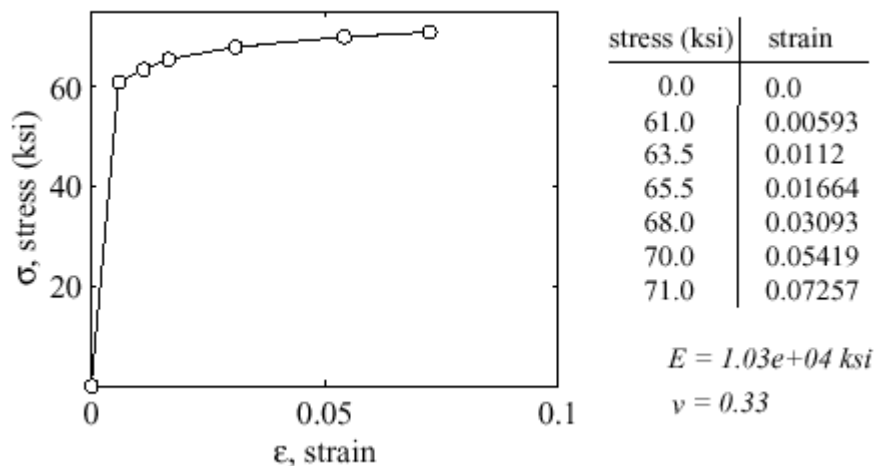


Figure FAC-2.5. Piecewise linear representation of uniaxial stress-strain relationship for 7075-T6 aluminum alloy used in the present example.

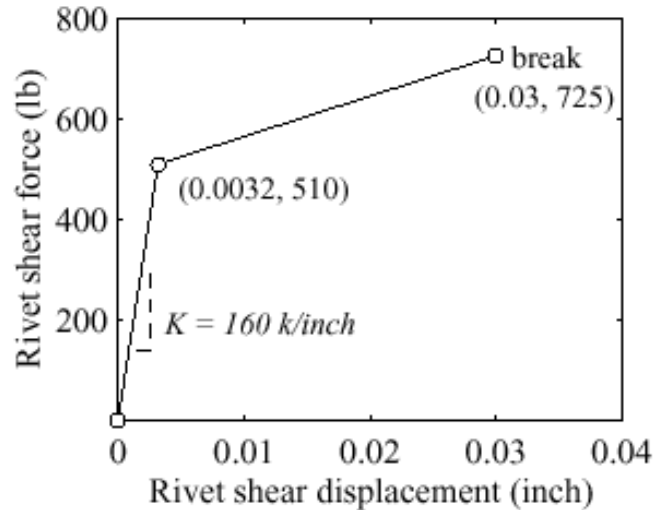


Figure FAC-2.6. Model for rivet shear stiffness and strength used in the present example.

Six different crack configurations with various lengths of lead and MSD cracks are studied. The initial configurations prior to crack growth are:

1. A 7.14 inch lead crack,
2. A 7.14 inch lead crack with 0.025 inch MSD cracks emanating from both sides of a fastener hole,
3. A 7.14 inch lead crack with 0.046 inch MSD cracks emanating from both sides of a fastener hole,
4. A 10 inch lead crack,
5. A 10 inch lead crack with 0.025 inch MSD cracks emanating from both sides of a fastener hole, and
6. A 10 inch lead crack with 0.046 inch MSD cracks emanating from both sides of a fastener hole.

The lead crack is located symmetrically about the central frame line. The MSD pattern is symmetric about the lead crack at the 3 rivets in front of the lead crack. The lead and MSD cracks are located along the upper rivet row in the upper skin of the joint. The crack configurations with a 10 inch initial lead crack are shown in [Figure FAC-2.7](#). Since rivet holes are not modeled explicitly in the finite element model, a small crack with a length equal to the rivet diameter plus the MSD length is used to model the MSD crack. The finite element mesh for the model is shown in [Figures FAC-2.8](#). [Figure FAC-2.9](#) shows details of the near-tip mesh pattern with the 0.04 inch crack tip elements used there. In addition to the effects of MSD, material thinning due to corrosion damage is also studied. The effect of material thinning is modeled by a uniform reduction in thickness of the upper skin at the lap joint in the two center bays.

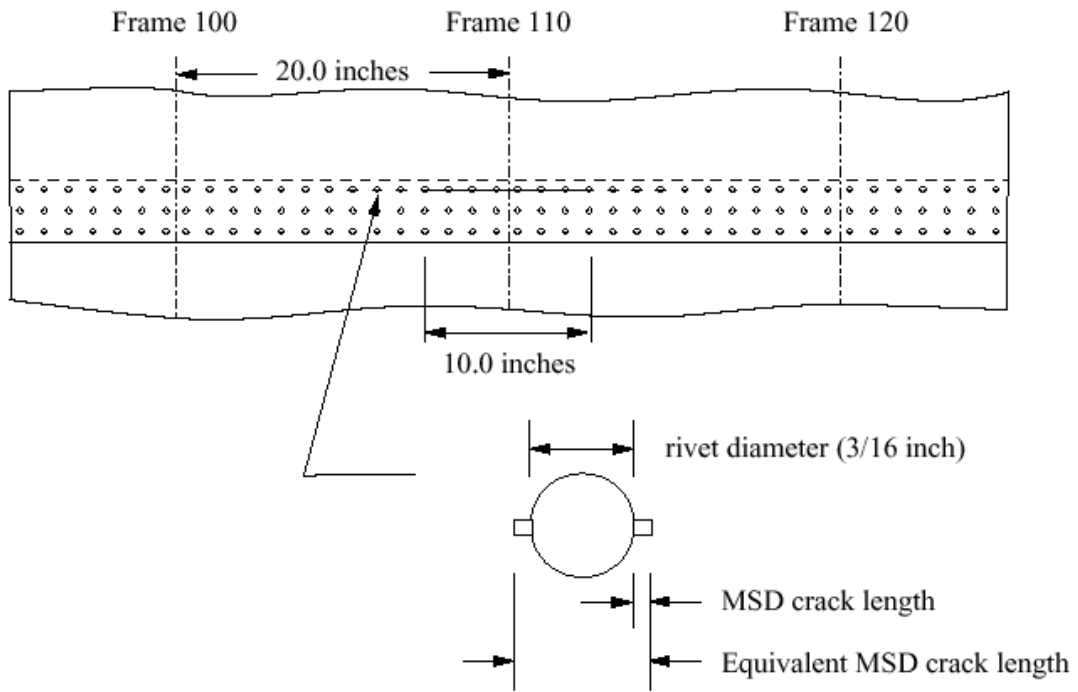


Figure FAC-2.7. Crack configurations for 10 inch lead crack and MSD.

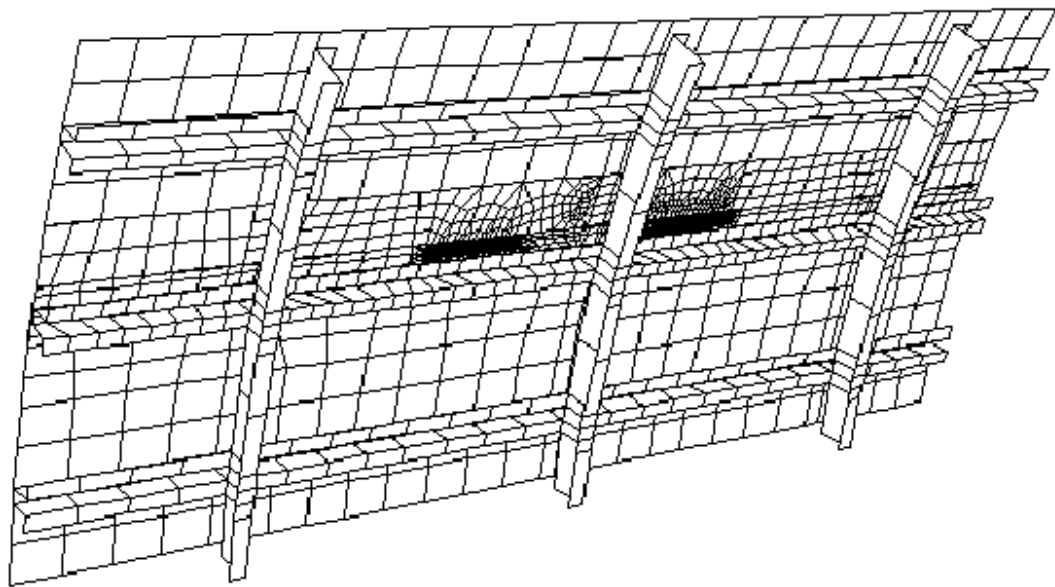


Figure FAC-2.8. Overall finite element mesh for present example.

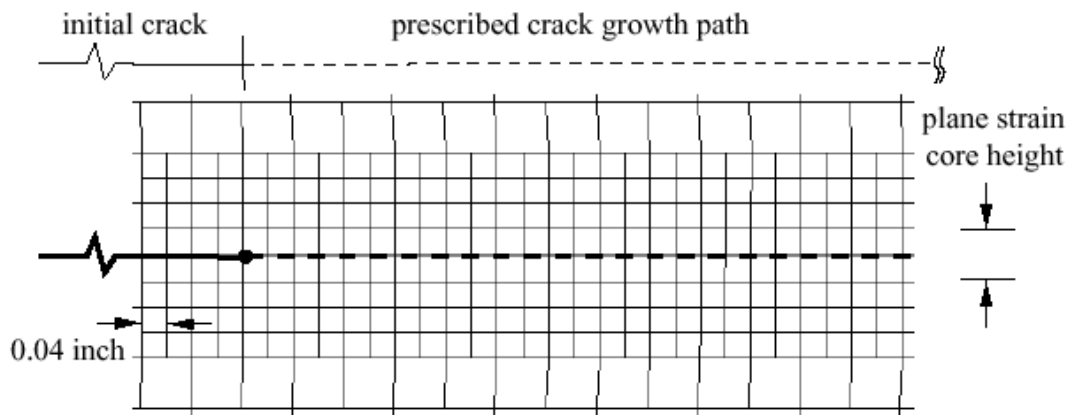


Figure FAC-2.9. Typical near-tip finite element meshing for present example.

Computational Results

[Figure FAC-2.10](#) shows the predicted results of the operating pressure loading versus the total crack extension for all the cases conducted in this study. The predicted residual strengths summarized in [Figure FAC-2.11](#) indicate:

- The MSD cracks significantly reduce the residual strength of the fuselage panel. A 21.8 to 28.0% loss of residual strength due to the presence of small MSD is observed.
- A 10% uniform thickness degradation due to corrosion damage reduces the residual strength by 3.4 to 9.0%. The coupling of MSD and corrosion damage leads to the most severe damage scenario.
- In general, increasing the lead and MSD crack lengths reduces the residual strengths. However, for the cases with a 10 inch initial lead crack, residual strength seems to be relatively insensitive to the MSD crack sizes.

The deformed structure at residual strength for the case with a 10 inch initial lead crack but without MSD and corrosion damage is shown in [Figure FAC-2.12](#). Out-of-plane bulging is observed in the skin crack edges. Because of the stiffness of the stringer, the bulging at the lower crack edge is much smaller than the opposing edge. The unsymmetric, out-of-plane bulging thus leads to an anti-symmetric bending deformation field at the crack tips [Potyondy 1995].

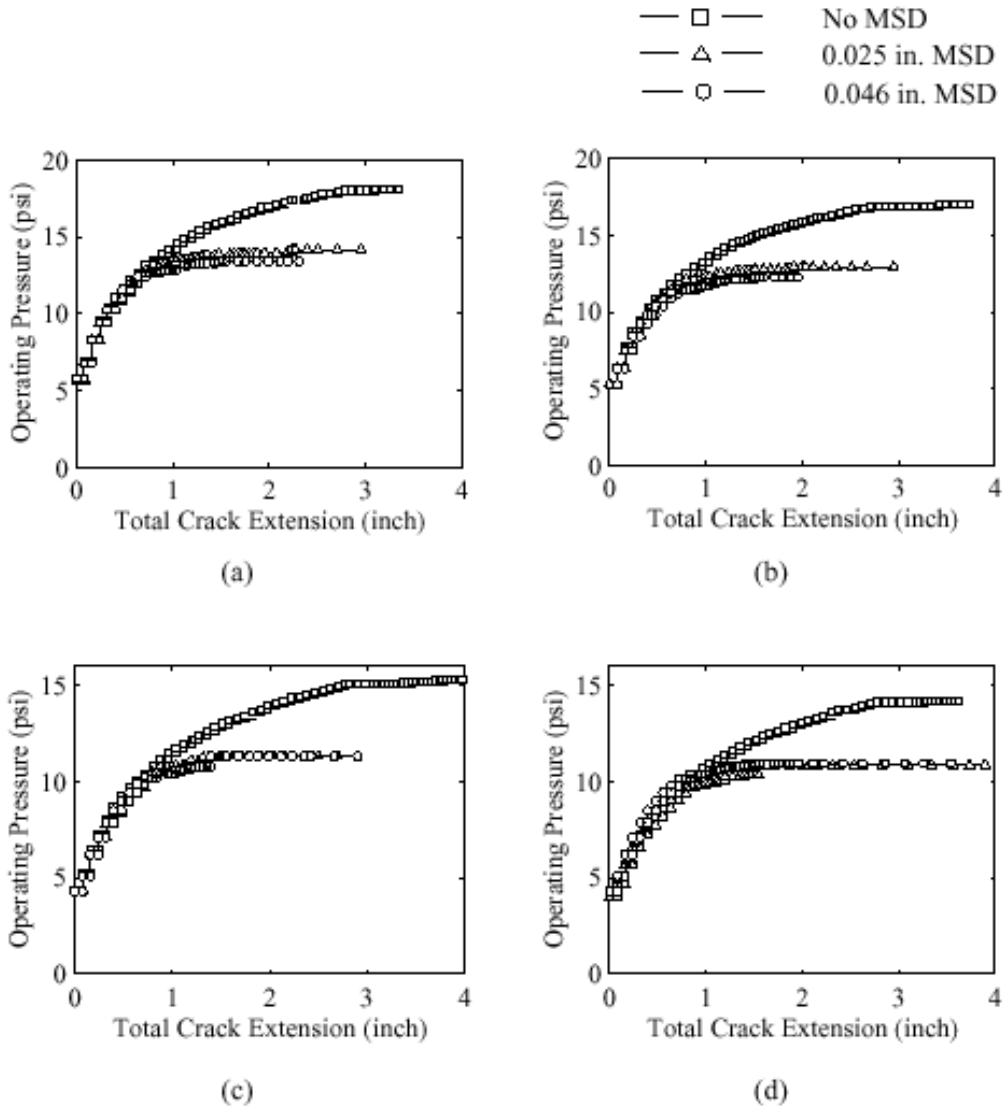


Figure FAC-2.10. Predicted operating pressure versus total crack extension for the present example: (a) 7.14 inch initial lead crack, (b) 7.14 inch initial lead crack with corrosion damage, (c) 10 inch initial lead crack, and (d) 10 inch initial lead crack with corrosion damage.

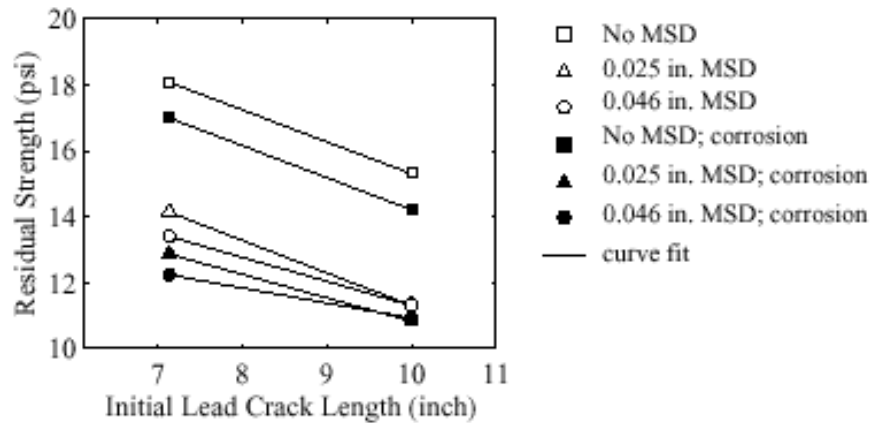


Figure FAC-2.11. Predicted residual strength versus initial lead crack length for present example.

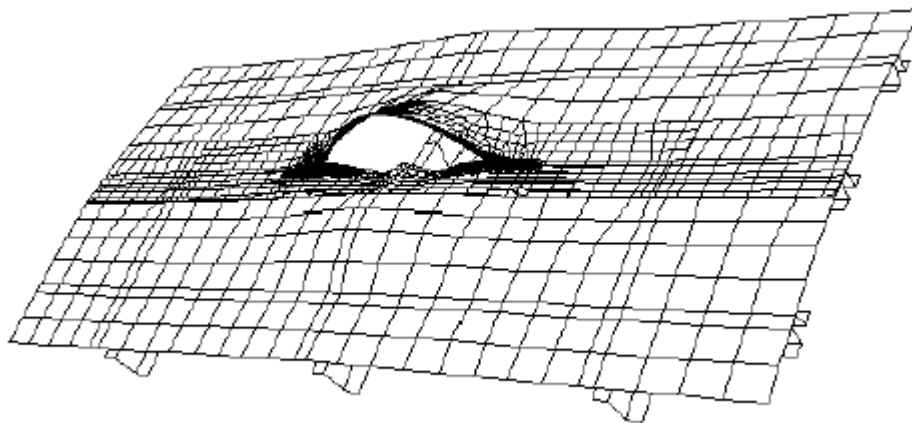


Figure FAC-2.12. Typical deformed shape of the present example (pressure = 15.3 psi, magnification factor = 5.0).

References

Cope, D., West, D., Luzar, J., Miller, G. Corrosion Damage Assessment Framework: Corrosion/Fatigue Effects on Structural Integrity. Technical Report D500-13008-1, The Boeing Defense and Space Group, 1998.

Dawicke, D., Piascik, R. and Newman, J. Prediction of Stable Tearing and Fracture of a 2000-Series Aluminum Alloy Plate Using a CTOA Criterion. In *Fracture Mechanics: 27th Volume, ASTM STP 1296*, Philadelphia, pp 90-104, 1997.

Dawicke, D. and Sutton, M. CTOA and Crack-tunneling Measurements in Thin Sheet 2024-T3 Aluminum Alloy. *Experimental Mechanics*, Volume 34, pp 357-368, 1994.

Nour-Omid, B. and Rankin, C. Finite Rotation Analysis and Consistent Linearization Using Projectors. *Computer Methods in Applied Mechanics and Engineering*, Volume 93, pp 353-384, 1991.

D. O. Potyondy, P. A. Wawrzynek, and A. R. Ingraffea. Discrete Crack Growth Analysis Methodology for Through Cracks in Pressurized Fuselage Structures. *International Journal for Numerical Methods in Engineering*, Volume 38, pp 1611-1633, 1995.

Rankin, C. and Brogan, F. The Computational Structural Mechanics Testbed Structural Element Processor ES5: STAGS Shell Element, 1991. NASA CR-4358.

Rankin, C., Brogan, F., Loden, W. and Cabiness, H. STAGS User Manual Version 2.4. Lockheed Martin Missiles & Space Co., Inc., Advanced Technology Center, 1997.

Riks, E. Some Computational Aspects of the Stability Analysis of Nonlinear Structures. *Computer Methods in Applied Mechanics and Engineering*, Volume 47, pp 219-259, 1984.

T. Swift. Fracture Analysis of Stiffened Structure. In *Damage Tolerance of Metallic Structures: Analysis Methods and Application*, ASTM STP 842, Philadelphia, pp 69-107, 1984.

R. D. Young, C. A. Rose, C. G. D'Avila, and J. H. Starnes, Jr. Crack Growth and Residual Strength Characteristics of Selected Flat Stiffened Aluminum Panels. *Proceedings of the First Joint DoD/FAA/NASA Conference on Aging Aircraft*, Ogden, Utah, July 1997.